First-principles electronic structure and relative stability of pyrite and marcasite: Implications for photovoltaic performance

Citation: Sun, Ruoshi, M. Chan, and G. Ceder. "First-principles Electronic Structure and Relative Stability of Pyrite and Marcasite: Implications for Photovoltaic Performance." Physical Review B 83.23 (2011) : 235311 ©2011 American Physical Society

As Published: http://dx.doi.org/10.1103/PhysRevB.83.235311

Publisher: American Physical Society

Persistent URL: http://hdl.handle.net/1721.1/65869

Version: Final published version: final published article, as it appeared in a journal, conference proceedings, or other formally published context

First-principles electronic structure and relative stability of pyrite and marcasite: Implications for photovoltaic performance

Ruoshi Sun,[1] M. K. Y. Chan,[1,2] and G. Ceder[1,*]

[1]*Department of Materials Science and Engineering, Massachusetts Institute of Technology, Cambridge, Massachusetts 02139, USA*

[2]*Center for Nanoscale Materials, Argonne National Laboratory, Argonne, Illinois 60439, USA*

(Received 13 February 2011; revised manuscript received 7 March 2011; published 8 June 2011)

Despite the many advantages (e.g., suitable band gap, exceptional optical absorptivity, earth abundance) of pyrite as a photovoltaic material, its low open-circuit voltage (OCV) has remained the biggest challenge preventing its use in practical devices. Two of the most widely accepted reasons for the cause of the low OCV are (i) Fermi level pinning due to intrinsic surface states that appear as gap states, and (ii) the presence of the metastable polymorph, marcasite. In this paper, we investigate these claims, via density-functional theory, by examining the electronic structure, bulk, surface, and interfacial energies of pyrite and marcasite. Regardless of whether the Hubbard U correction is applied, the intrinsic {100} surface states are found to be of d_{z^2} character, as expected from ligand field theory. However, they are not gap states but rather located at the conduction-band edge. Thus, ligand field splitting at the symmetry-broken surface cannot be the sole cause of the low OCV. We also investigate epitaxial growth of marcasite on pyrite. Based on the surface, interfacial, and strain energies of pyrite and marcasite, we find from our model that only one layer of epitaxial growth of marcasite is thermodynamically favorable. Within all methods used (LDA, GGA-PBE, GGA-PBE+U, GGA-AM05, GGA-AM05+U, HSE06, and Δ-sol), the marcasite band gap is not less than the pyrite band gap, and is even larger than the experimental marcasite gap. Moreover, gap states are not observed at the pyrite-marcasite interface. We conclude that intrinsic surface states or the presence of marcasite are unlikely to undermine the photovoltaic performance of pyrite.

DOI: 10.1103/PhysRevB.83.235311 PACS number(s): 71.20.Nr, 68.35.bg, 81.15.Aa

I. INTRODUCTION

In many respects, pyrite is a promising photovoltaic material due to its earth abundance,[1] nontoxic elements, suitable band gap (0.95 eV),[2] and, most importantly, its excellent optical absorptivity.[3] Although it is an indirect-gap material, its optical-absorption coefficient within the visible light spectrum is on the order of 10^5 cm^{-1},[2] outperforming silicon by two orders of magnitude and even direct-gap materials such as GaAs. In a recent cost analysis for large-scale photovoltaic applications, pyrite is ranked number one among all practical or promising thin-film solar cell materials.[4] However, experiments in the mid-1980s and 1990s show a persistently low open-circuit voltage (OCV) of around 200 mV, which is the primary factor that reduces the efficiency of pyrite photoelectrochemical cells to 2%.[2] Thus, it is important to understand what limits the OCV and how it can be enhanced.

There have been many proposals in the literature regarding the cause of the low OCV in pyrite. They can be classified into three main categories: (i) Intrinsic surface states. Bronold and co-workers have suggested that intrinsic {100} surface states appear as gap states, thereby pinning the Fermi level.[2,5–8] (ii) Presence of marcasite. Wadia and co-workers have suggested that trace amounts of marcasite, a polymorph of pyrite with a significantly lower band gap, would deteriorate the photovoltaic performance of pyrite.[9,10] (iii) Defects. Various research groups have suggested that electronic states can be introduced into the band gap due to intrinsic defects such as bulk sulfur vacancies[11,12] and surface sulfur vacancies.[13] Abd El Halim *et al.* have also suggested the possibility of line defects and extrinsic point defects.[14] Oertel *et al.* have attributed the poor performance to the limitation of carrier transport by trap states at grain boundaries.[15] In this study, we mainly focus on the possible role of surface states (i) and marcasite formation (ii). Our results question these explanations for the low OCV. The effect of defects (iii) shall be considered in a forthcoming study.

In Sec. II, we will first examine the pyrite and marcasite crystal structures, their similarities, and the possibility of marcasite epitaxial growth on pyrite, followed by more detailed discussions on the different proposed causes for the low OCV of pyrite. First-principles computational details will be presented in Sec. III. In Sec. IV, we will discuss surface energies and electronic structure calculations of pyrite, as they are related to the intrinsic surface-state hypothesis (i). In Sec. V, the thermodynamic epitaxial growth condition of marcasite on pyrite, and the electronic structures of the bulk phases and the pyrite-marcasite interface, will be analyzed to investigate the marcasite hypothesis (ii).

II. BACKGROUND

A. Pyrite crystal structure

The formula unit of pyrite is FeS_2, where the oxidation states of Fe and S are +II and −I, respectively.[16] The structure belongs to the space group $Pa\bar{3}$. The conventional unit cell is shown in Fig. 1. Fe atoms are located at face-centered-cubic (fcc) sites, whereas S atoms form distorted octahedra around Fe. The positions of all the S atoms can be described by a single Wyckoff parameter, u. These positions are $\pm(u,u,u)$, $\pm(\frac{1}{2}+u,u,\frac{1}{2}-u)$, $\pm(u,\frac{1}{2}-u,\frac{1}{2}+u)$, and $\pm(\frac{1}{2}-u,\frac{1}{2}+u,u)$. Each S atom is tetrahedrally coordinated by three Fe atoms and one S atom, with which the S_2 dimer is formed.[1] The centers of the S_2 dimers form an fcc sublattice that interpenetrates the Fe sublattice. Thus, the pyrite structure can be viewed as a

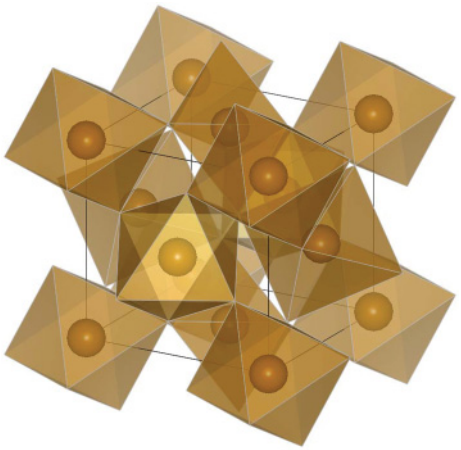

FIG. 1. (Color online) Unit cell of pyrite FeS_2 (rendered by VESTA[17]). The spheres at fcc sites are Fe atoms. Each Fe atom sits in a slightly distorted octahedral environment of S atoms, which are located at the octahedral vertices.

slight modification of the NaCl structure, such that each Cl site is occupied by ⟨111⟩-oriented S_2 dumbbells.

It is well-known from crystal-field theory that the energies of transition-metal d orbitals are nondegenerate within an octahedral environment.[18] Specifically for FeS_2, the triply degenerate d_{xy}, d_{yz}, and d_{xz} states, collectively known as t_{2g}, dominate the valence band (VB), whereas the doubly degenerate d_{z^2} and $d_{x^2-y^2}$ states, collectively known as e_g, dominate the conduction band (CB). Both pyrite and marcasite are low-spin (LS) semiconductors because their t_{2g} levels are fully occupied by the six Fe d electrons.[19] The ligand field theory of various materials that have the pyrite or marcasite crystal structure is discussed in Ref. 19.

B. Similarity of pyrite and marcasite crystal structures

Marcasite forms an orthorhombic *Pnnm* structure with unit cell shown in Fig. 2. Note the octahedral environment around the body-centered Fe atom. By repeating the unit cell, one can see that the octahedra in marcasite are edge-shared, whereas those in pyrite are corner-shared (Fig. 1). Experimentally, the lattice constant of pyrite is $a = 5.416$ Å;[1] the lattice constants of marcasite are $a = 4.443$ Å, $b = 5.425$ Å, and $c = 3.387$ Å.[20] Note that the b constant and the [101] length ($\sqrt{a^2 + c^2} = 5.587$ Å) of marcasite are similar to the pyrite lattice constant, with lattice mismatches of 0.2% and 3%, respectively. The structural relationship between the different octahedra linkages in pyrite and marcasite is discussed in Ref. 21. The pyrite-marcasite structural transformation can be described by a rotation of Fe-S chains in alternating layers of the (101) marcasite plane, as discussed in Ref. 22. Indeed, due to their structural similarities, intergrowth (epitaxial growth) of marcasite in (on) pyrite has been widely observed.[9,23–25] The thermodynamic conditions for such growth behavior will be discussed in later sections.

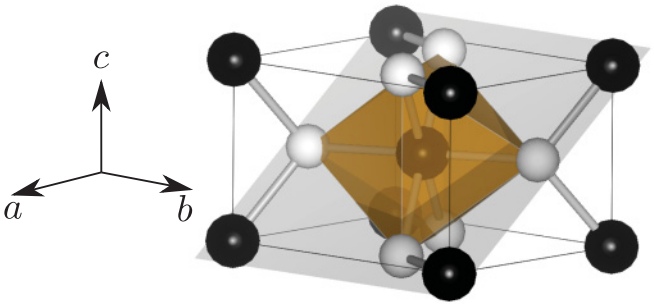

FIG. 2. (Color online) Unit cell of marcasite FeS_2 (rendered by VESTA[17]). Black (white) spheres represent Fe (S) atoms. The (101) plane is highlighted in gray. The octahedra is edge-shared by the S atoms on the (001) faces.

C. Proposed causes for low OCV of pyrite

1. Intrinsic surface states

Figure 3 shows the (100) surface of pyrite. Of the three possible terminations, only one is nonpolar. [S-Fe-S] patterns repeat along the surface normal direction in Fig. 3a. Polar surfaces are created from the terminations that yield [S-S-Fe] or [Fe-S-S] as the three layers nearest to the surface. In the nonpolar surface, ending as [S-Fe-S], the coordination number of a surface Fe atom is 5, being 1 lower than that of a bulk Fe atom. The local coordination of S around Fe is reduced from octahedral to square pyramidal, as illustrated in Fig. 3b.

The ligand field model developed by Bronold *et al.* to describe the local electronic structure is shown schematically in Fig. 4.[5] Bronold *et al.* estimate the octahedral splitting energy 10 Dq to be 2 eV based on the centers of mass of

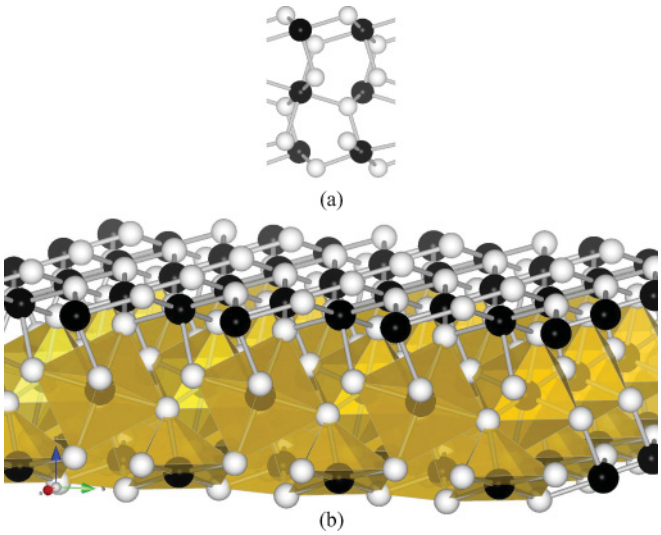

FIG. 3. (Color online) (a) Side view of the unique nonpolar pyrite (100) surface. Looking along the surface normal direction (upwards), the atomic layers have the repetitive pattern [S-Fe-S]. Other possible terminations result in repeating layers of [S-S-Fe] or [Fe-S-S]. In both cases, polar surfaces result. Hence, this S-terminated surface is the only possible nonpolar (100) surface. In (b), note the octahedral environment around bulk Fe atoms, and the square pyramidal environment around surface Fe atoms. Polyhedra are not shown in the topmost layer. Black (white) spheres are Fe (S) atoms. (Rendered by VESTA.[17])

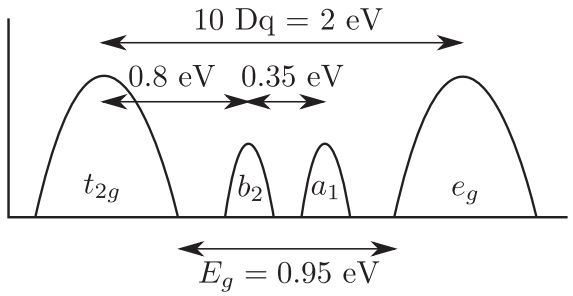

FIG. 4. Schematic of the ligand field model developed by Bronold *et al*.[5] The CB and VB are dominated by e_g and t_{2g} states, respectively. As a result of symmetry reduction, a_1 and b_2 states, which correspond to d_{z^2} and d_{xy} states, are introduced within the band gap.

the CB and VB density of states (DOS) in the electronic structure calculation by Folkerts *et al*.[26] Using the splitting energies of the square pyramidal configuration ($d_{x^2-y^2}$ at 9.14 Dq; d_{z^2},d_{xy} at ±0.86 Dq; d_{xz},d_{yz} at −4.57 Dq) calculated by Krishnamurthy and Schaap,[18] they claim that the d_{z^2} and d_{xy} states are split off from the e_g and t_{2g} states in the CB and VB, respectively, thereby introducing two gap states a_1 and b_2.[5] It should be pointed out that the splitting energies are greatly influenced by the choice of a free parameter ρ.[18] Without justification, Bronold *et al*. implicitly assume $\rho = 2$ in their model. For this particular choice of ρ, gap states are centered at 4 Dq (0.8 eV) above the center of mass of the t_{2g} states in the VB and separated from each other by 1.7 Dq (0.35 eV). They suggest that the Fermi level is pinned by these states, hence reducing the OCV. As the Bronold model is not free of parameters, we will examine the claims of gap states by direct *ab initio* electronic structure calculations in this paper.

2. *Presence of marcasite*

Phase purity is a critical issue in photovoltaic devices, especially if secondary phases have a lower band gap than the host material, or if they introduce interfacial states within the band gap that may lead to Fermi level pinning. For instance, due to its metallic character, trace amounts of the Fe-deficient pyrrhotite phase ($Fe_{1-x}S$) are detrimental to the photovoltaic performance of pyrite.[25] Thomas *et al*. have shown that there exists a critical S partial pressure above which growth of pyrrhotite can be avoided.[25] Since pyrrhotite is not commonly reported to intergrow with pyrite, and the means to prevent its growth have been developed, the pyrrhotite phase will not be examined in this study.

Another cause for the low OCV of pyrite is attributed to the presence of its polymorph, marcasite.[9] Intergrowth of these two phases has been widely reported (see, e.g., Refs. 9,24,25). In addition, epitaxial overgrowth of marcasite (101) on pyrite (100) has been observed from natural samples.[22] While there has been no study on the mechanism of how marcasite may affect the photovoltaic performance of pyrite, it has been speculated that the lower gap of marcasite plays a role. There is only one published experimental value of the band gap of marcasite (0.34 eV), which is much lower than that of pyrite. This value is obtained using resistivity measurements with the assumption that the carrier mobility is dominated by lattice scattering.[27] As far as the authors are aware, there are no other reports on the gap of marcasite and its value has never been verified via a more reliable and direct method such as optical measurements. Intuitively, one may reason that marcasite should have a lower gap than pyrite, because marcasite has lower symmetry compared to pyrite, and hence enhanced crystal-field splitting.[28] Nonetheless, there is no direct, unambiguous evidence that marcasite has a lower gap than pyrite.

To model the pyrite-marcasite system, one should first understand their relative stability. From calorimetric measurements, pyrite is the ground-state phase within 5–700 K, and the marcasite-to-pyrite phase transformation is found to be exothermic.[20] Computationally, Spagnoli *et al*. find that the relative phase stability depends on the exchange-correlation functional: while marcasite is the ground state within the local density approximation (LDA) and the generalized gradient approximation (GGA) within the Perdew-Burke-Ernzerhof formulation (PBE), pyrite is more stable within recently developed GGA functionals such as AM05, Wu-Cohen, and PBEsol.[10] There has been no prior computational work on the thermodynamic stability of epitaxial growth of marcasite on pyrite. Whether interfacial states are introduced into the pyrite band gap by marcasite is also unknown. All of the above issues will be addressed in this work.

III. DETAILS OF FIRST-PRINCIPLES COMPUTATIONS

Density-functional theory (DFT)[29,30] calculations with projector augmented wave (PAW) potentials[31,32] were performed using the plane-wave code Vienna Ab-initio Simulation Package (VASP)[33–36] We used both the LDA[37] and the GGA to the exchange-correlation functional. Two formulations of GGA, namely, PBE[38,39] and AM05,[40,41] were adopted. The spin states of pyrite and marcasite were determined from spin-polarized DFT calculations.[42,43] In cases in which the Hubbard U correction within the Liechtenstein scheme[44] was applied to GGA calculations, we chose the parameters $U = 3$ eV and $J = 1$ eV that correctly predict the high spin state of Fe under negative pressure, as discussed in Ref. 45.

The plane-wave energy cutoff was 350 eV for all calculations. Within each self-consistency cycle, the total energy was converged to within 10^{-6} eV. Forces in ionic relaxations were converged to within 0.01 eV/Å. Convergence tests with respect to energy cutoff, Monkhorst-Pack[46] k-point density, supercell size and vacuum size were performed such that surface and interfacial energies were converged to within 0.01 J/m^2. For bulk reference energies, we used a k-mesh of $8 \times 8 \times 8$ for pyrite (12-atom unit cell) and $8 \times 6 \times 10$ for marcasite (6-atom unit cell). Kohn-Sham gaps were computed using a Γ-centered k-mesh of $16 \times 16 \times 16$ for pyrite and $16 \times 12 \times 20$ for marcasite. Band structures were obtained from subsequent non-self-consistent calculations with $15-k$ points per high-symmetry line. For surface and interfacial calculations, we used a k-mesh of $4 \times 4 \times 1$. Surface terminations were chosen to generate nonpolar supercells, avoiding dipole effects under periodic boundary conditions (see Ref. 47 for details). Details of the approach used to obtain surface and interfacial energies converged with respect to slab and vacuum sizes can be found in Appendix A. At convergence, the (100), (110), (111), and (210) pyrite slabs contained 24, 48, 72,

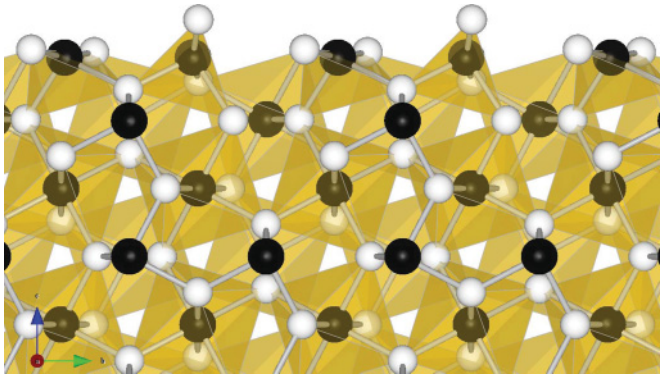

FIG. 5. (Color online) Side view of pyrite (110) surface (rendered by VESTA[17]). Black (white) spheres are Fe (S) atoms. The surface is nonpolar and S-terminated.

and 60 atoms, respectively. Supercells of the pyrite-marcasite interface contained 36 to 120 atoms.

IV. INTRINSIC PYRITE (100) SURFACE

We divide our results into two parts. In this section, we present the surface energies of pyrite (Sec. IV A) and electronic densities of states (DOS) for the dominant surface (Sec. IV B). We compare our first-principles calculations with the ligand field calculations of Bronold *et al.*[5] In Sec. V, we first show how the bulk, surface, interfacial, and strain energies of pyrite and marcasite are used in an energy model to predict whether epitaxial growth of marcasite on pyrite is thermodynamically favorable (Secs. V A and V B). We then examine the electronic structures of marcasite and at the pyrite-marcasite interface to verify whether marcasite can undermine the OCV of pyrite (Secs. V C and V D).

A. Surface energies

The most commonly observed surfaces of pyrite are {100}, {110}, {111}, and {210}.[1] Figures 3, 5, 6, and 7 show the corresponding structures. A detailed description of the structures of these surfaces can be found in Refs. 48–50. The

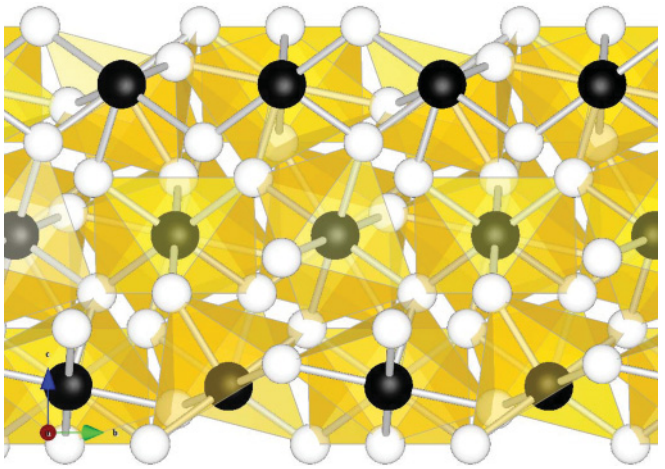

FIG. 6. (Color online) Side view of pyrite (111) surface (rendered by VESTA[17]). Black (white) spheres are Fe (S) atoms. The surface is nonpolar and S-terminated.

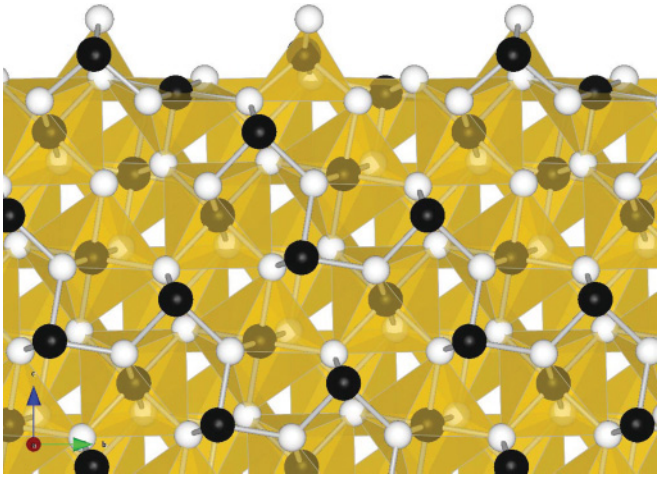

FIG. 7. (Color online) Side view of pyrite (210) surface (rendered by VESTA[17]). Black (white) spheres are Fe (S) atoms. The surface is nonpolar and S-terminated.

surface energies are calculated via Eq. (A1) in Appendix A. For all functionals used, the {100} surface has the lowest energy, as shown in Table I. Our PBE surface energies agree well with another first-principles investigation by Hung *et al.*, who used the same exchange-correlation functional.[48,49] We observe that the surface energies are lowest in PBE, followed by AM05, and largest in the LDA. However, the relative magnitudes are consistent across functionals. The Wulff shape, i.e., the equilibrium shape of a single crystal, of pyrite is shown in Fig. 8. Besides the dominant {100} surface, only {111} facets are observed. Hence, the minimum-energy structure of pyrite is the cubo-octahedral structure. Since the relative surface energies are similar for different functionals, the predicted Wulff shape is independent of the functional used, despite significant functional dependence of the surface energies themselves.

B. Surface states

As {100} is the dominant surface, we investigate the surface states of this facet. To obtain the exact character of the surface states, the coordinate frame is rotated into the Fe-S bonds prior to projection onto partial d states.[51] The DOS of bulk pyrite and the (100) surface are compared in Fig. 9. For bulk pyrite, the Kohn-Sham gap is 0.40 eV within PBE. The tail in the CB is due to an S p state. The VB and CB are dominated by t_{2g} and e_g states, respectively (not shown), agreeing with ligand field theory.[19] For the (100) surface, we only observe a pronounced d_{z^2} state that is pulled down from the conduction-band manifold of e_g states, but not inside the gap. The d_{xy} gap

TABLE I. Relaxed surface energies (in J/m^2) of pyrite FeS_2. PBE results are compared with Refs. 48 and 49, where PBE was used. AM05 energies for (111) and (210) surfaces are not available due to convergence issues.

Surface	LDA	AM05	PBE	Hung *et al.*[48,49]
(100)	1.58	1.26	1.04	1.06
(110)	2.38	2.02	1.72	1.68
(111)	2.01	-	1.43	1.40
(210)	2.13	-	1.49	1.50

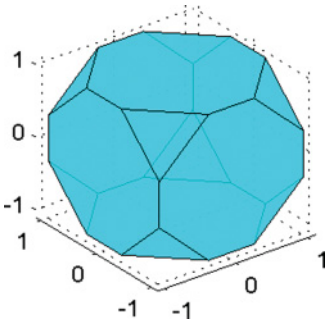

FIG. 8. (Color online) Wulff shape of pyrite within the GGA-PBE. Surface energies are taken from Table I. The dominant surface is {100}. {111} facets are also observed. The equilibrium shape is cubo-octahedral.

state predicted by Bronold *et al.*[5] is not seen. We have also performed the same calculation within the LDA and AM05. However, gap states are not found.

1. Hubbard U correction

One may question whether the intrinsic surface states would become gap states if the band gap were more accurately calculated, since the Kohn-Sham (KS) gap obtained with local and semilocal functionals severely underestimates the band gap. Hence, it may be desirable to apply a Hubbard U correction, which has been shown to be successful in transition-metal electronic structure calculations. (See, e.g., Refs. 52 and 53.) However, as the surface states and CB states are of d character, we expect that the same qualitative results should be obtained within GGA+U. To verify, we perform PBE + U calculations, following Persson *et al.* for the choice of U and J. The effective $U = 2$ eV is chosen to correctly predict a pressure-induced spin transition.[45] Fe^{2+} in pyrite has a d^6 electronic configuration; pyrite is both expected and observed to be low spin.[19] We verify that the LS configuration

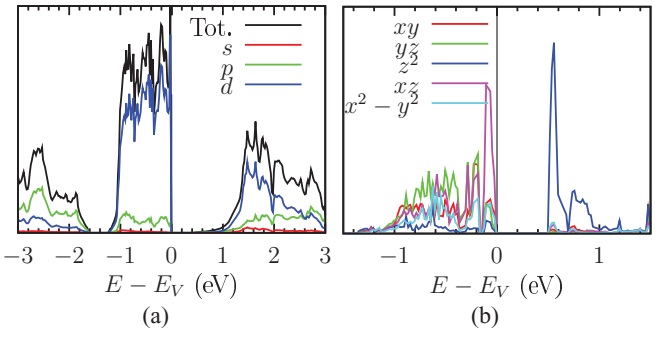

FIG. 9. (Color online) GGA-PBE DOS of pyrite (a) bulk, (b) (100) surface. In (a), both the total DOS and s-p-d decomposed DOS are shown. The CB and VB are dominated by Fe d states. We have verified that these d states within the CB and VB are e_g and t_{2g}, respectively. Due to the presence of an S p state, the CB tail extends to 0.4 eV above the VB edge. In (b), the DOS of d orbitals are shown to identify the character of intrinsic surface states. The intrinsic surface state appears at the CB edge, not within the band gap, and is of d_{z^2} character. However, ligand field splitting in the VB is not observed and d_{xy} surface states are not found, contrary to the prediction of Bronold and co-workers.[5]

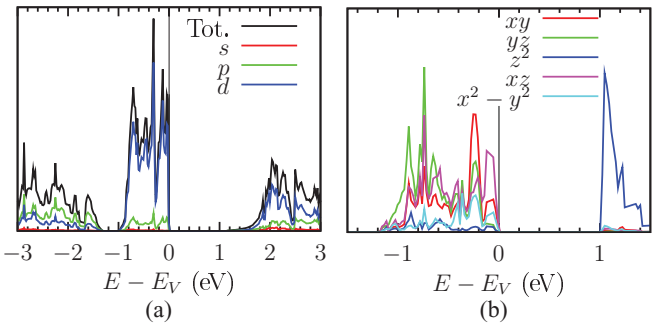

FIG. 10. (Color online) PBE+U DOS of pyrite (a) bulk, (b) (100) surface. In (a), both the total DOS and the s-p-d decomposed DOS are shown. The PBE+U gap of bulk pyrite is 1.03 eV. In (b), the DOS of d orbitals are shown to identify the character of intrinsic surface states. Similar to Fig. 9(b), a d_{z^2} surface state is found at the CB edge. Gap states are not observed.

is the ground state within both PBE and PBE + U. By applying the Hubbard U correction to pyrite in the LS configuration, the KS gap is increased to 1 eV, which coincides with the experimental band gap. We emphasize that the U value is not fitted to the band gap.

Since the conduction band is dominated by d states, we expect it to shift upward with respect to the VB edge. Moreover, as the intrinsic surface states at the conduction band minimum (CBM) are also d states, they should move along with the CB. We verify that these intrinsic surface states are not gap states within PBE + U. As shown in Fig. 10, intrinsic surface states and the CB are shifted by the same amount, as compared to PBE. The d_{z^2} surface states are still located at the CB edge, and no gap states are found.

From the above discussion, we observe several discrepancies between first-principles calculations and the Bronold model.[5] First, the Bronold model predicts two types of intrinsic surface states; however, only the d_{z^2} surface state is observed within DFT. Within the VB, the predicted d_{xy} state is not observed to move toward the band edge. The fact that the t_{2g} states remain fairly degenerate at the symmetry-broken surface suggests that applying the parameters from the simplified model of Krishnamurthy and Schaap[18] is inadequate to capture the physics of the electronic structural properties of the pyrite (100) surface. Second, the Bronold model predicts that these surface states are gap states, leading to Fermi level pinning and undermining the photovoltaic performance of pyrite; however, the surface states are not found within the band gap, regardless of the exchange functional used and whether or not we apply the Hubbard U correction. Therefore, we conclude that intrinsic surface states are unlikely to be the cause of the low OCV in pyrite.

V. PYRITE AND MARCASITE

A. Model for epitaxial growth of marcasite on pyrite

Epitaxial growth of marcasite (101) on pyrite (100) is shown schematically in Fig. 11. The condition for marcasite growth on pyrite to be energetically favorable is

$$A(\gamma_{pm} + \gamma_{mv} - \gamma_{pv}) + N\Delta g < 0, \quad (1)$$

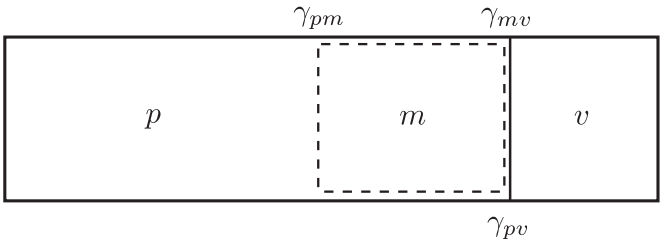

FIG. 11. Schematic of marcasite overgrowth on pyrite. Pyrite, marcasite, and vacuum are labeled as p, m, and v, respectively. By growing marcasite (enclosed in the dashed region), the top bulk layers of pyrite are replaced, resulting in a difference in bulk energy Δg. Moreover, the pyrite (001) surface energy γ_{pv} is replaced with the marcasite (101) surface energy γ_{mv} plus an interfacial energy between the two phases γ_{pm}.

where γ is the surface or interfacial energy between marcasite (101) (m), pyrite (100) (p), and/or vacuum (v), N is the number of layers of marcasite (number of S-Fe-S stacking motifs along the z direction), Δg is the magnitude of the free-energy difference between the pyrite and marcasite phases per layer, and A is the cross-sectional area. From this energy balance equation, the critical N can be calculated for a given set of surface and interfacial energies.

B. Possibility of marcasite epitaxial growth on pyrite

Different pyrite (100)–marcasite (101) interfaces can be created depending on the orientation angle θ and the parity of the number of layers. (We use the Fiorentini-Methfessel method[54] extended for interfacial energies as presented in Appendix A.) We match the two phases such that $[101]_m \parallel [100]_p$, and perform integer multiples of 90° rotations of the marcasite phase relative to the pyrite phase about the normal to the interface (which will henceforth be referred to as the z direction), to generate four supercells. We denote the rotation angle as θ. From Fig. 3, we see that the pyrite unit cell consists of six monolayers, which can be subdivided into two distinct groups of S-Fe-S layers. The number of S-Fe-S layers along the z direction shall be denoted as N. The six monolayers in a marcasite (101) cell can also be subdivided into two S-Fe-S layers, but they are identical by translational symmetry because the marcasite (101) cell has twice the volume of the marcasite unit cell. Therefore, different pyrite-marcasite interfaces result from N even or odd, for a fixed θ. Figure 12 illustrates how the parity of N can generate different pyrite-marcasite interfaces under periodic boundary conditions. In Fig. 12(a), octahedra are edge-shared across both interfaces within the supercell. Thus we denote the total interfacial energy by $\gamma_{pm} = 2\gamma_e$, where the subscript e stands for "edge." In Fig. 12(b), octahedra are corner-shared at one interface and edge-shared at the other. The total interfacial energy is $\gamma_{pm} = \gamma_e + \gamma_c$, where the subscript c stands for "corner." Calculations are performed for $N = 3,4,\ldots,10$.

Figure 13 shows that the interfacial energy is indeed dependent on θ and the parity of N. The 0° and 180° configurations are the same, so the energies are exactly identical. Also, notice that the interfacial energy for the 0° and 180° configurations is constant with respect to the parity of N, unlike the 90° and 270° scenarios. The lowest-energy

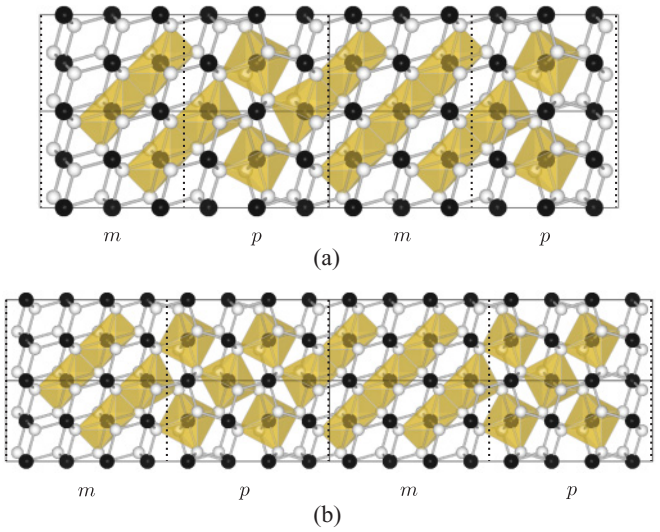

FIG. 12. (Color online) Structures of the pyrite (001)–marcasite (101) interface for $\theta = 270°$ and (a) $N = 3$, (b) $N = 4$ (rendered by VESTA[17]). Black (white) spheres are Fe (S) atoms. Pyrite and marcasite phases are labeled by p and m, respectively, where the interfaces are marked by vertical dotted lines. For clarity, the supercell (enclosed in a black rectangle) is repeated along the [010] (downward) and [001] (rightward) directions, and octahedra are drawn for Fe atoms in the innermost layer only. Note the octahedra are edge-sharing in bulk marcasite but corner-sharing in bulk pyrite. At the interface, the octahedra are edge-sharing when N is odd (a), but can be corner-sharing when N is even [from left to right, the second dotted line in (b)], showing that different interfacial energies may result depending on the parity of N. Consecutive 90° rotations of one phase with respect to the other about the rightward axis can create more variations (not shown). It is verified that the corner-sharing-type interface with $\theta = 270°$ is the most energetically favorable.

configuration is achieved when N is even and $\theta = 270°$, due to the presence of corner-shared octahedra across the interface. Based on the converged interfacial energies for N even and odd, we obtain that $2\gamma_e = 1.12\ \mathrm{J/m^2}$ and $\gamma_e + \gamma_c = -0.48\ \mathrm{J/m^2}$, where γ_e and γ_c are the edge-shared and corner-shared interfacial energies, respectively. By solving these equations, we get $\gamma_e = 0.56\ \mathrm{J/m^2}$ and $\gamma_c = -1.04\ \mathrm{J/m^2}$.

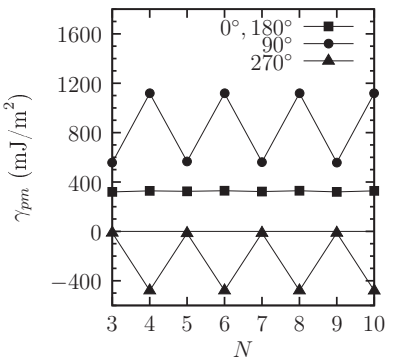

FIG. 13. The pyrite (100)–marcasite (101) interfacial energy, γ_{pm}, within the GGA-PBE. The interfacial energy depends on the relative orientation between the two phases and the parity of N.

TABLE II. Bulk energies (in meV/FU) of pyrite (p) and marcasite (m) referenced to the strain-free marcasite total energy. Strain energies of marcasite are calculated under epitaxial and periodic boundary conditions, as discussed in the main text.

Phase	Strain	LDA	PBE	PBE+U	AM05
p	0	−8.4	21.6	26.7	−8.8
m	0	0	0	0	0
m	ϵ_{ep}	898.3	859.8	865.6	896.7

We remark that the negative interfacial energy is not an artifact, but is due to the strain energy as a result of imposing interfacial coherency. In the energy-balance equation [Eq. (1)], the strain energy is included in the Δg term instead:

$$\Delta g = g_m - g_p = [g_m(\epsilon = \epsilon_{ep}) - g_m(\epsilon = 0)] + [g_m(\epsilon = 0) - g_p]. \quad (2)$$

Here the energy difference in the first set of brackets is the strain energy for marcasite epitaxial growth on pyrite; ϵ is the strain in the marcasite phase and ϵ_{ep} represents the epitaxial strain conditions: (i) $a' \equiv \sqrt{a_m^2 + c_m^2} = a_p$, where subscripts m and p denote the marcasite and pyrite phases, respectively; (ii) $b_m = a_p$; (iii) shearing along $[\bar{1}01]$ such that [101] becomes normal to the (101) plane, which is necessary to satisfy periodic boundary conditions. Conditions (i) and (ii) impose lattice mismatches of 3% and 0.1%, respectively, within PBE. (For lattice constants in other functionals, see Appendix B.) The third condition is equivalent to setting the c/a ratio to 1, since the angle between the (101) plane and the [101] direction is equal to $\cos^{-1}\frac{(c/a)^2-1}{(c/a)^2+1}$. The energy difference in the second set of brackets is the relative phase stability between pyrite and marcasite. In Appendix B, we show that the ground-state phase is functional- and volume-dependent.

Total energies of pyrite and strained marcasite referenced to the strain-free marcasite phase are shown in Table II. The magnitude of the difference in the first set of brackets in Eq. (2) (marcasite strain energy) is much larger than that in the second set (relative phase stability) for all functionals used. Although different functionals give different predictions for the ground-state phase [sign of $g_m(\epsilon = 0) - g_p$], the strain energy required for epitaxial growth is one order of magnitude higher than the strain-free bulk energy difference [$O(100)$ compared to $O(10)$ meV/FU]. Substituting the PBE bulk, surface, and interfacial energies into Eq. (1), we find that the thermodynamic condition for marcasite epitaxial growth is $N < 1.5$, which means that the critical N is only 1 for the corner-shared-type interface. We also find the same result using other functionals, as the marcasite strain energy is much more significant than the bulk energy difference between strain-free marcasite and pyrite. It is emphasized that the parity of N determines whether the corner-sharing-type interface is present in the supercell under periodic boundary conditions. It does not mean that marcasite can only grow by an even or odd number of layers.

Since the critical N is so small, we cross-validate our prediction via direct computation of pyrite-marcasite-vacuum supercells, as depicted schematically in Fig. 11. As the pyrite-marcasite system is separated from its periodic image by a layer of vacuum in the z direction, there is only one pyrite-marcasite interface here. Calculations are performed for $N = 1, 2, 4, 6,$ and 8 layers of marcasite on top of pyrite, where the interface is of the corner-sharing type and $\theta = 270°$ (lowest-energy configuration). The total energy (per formula unit) is shown in Fig. 14. In this direct approach, we find a critical N of 2. The discrepancy between the predicted value of one layer may be attributed to additional ionic relaxation within the marcasite layer to reduce the strain energy, thereby (marginally) enhancing growth. With the qualitative consistency between the two approaches, we have shown that epitaxial growth of marcasite on pyrite is thermodynamically favorable, but only limited to a few layers, as further growth becomes energetically unfavorable.

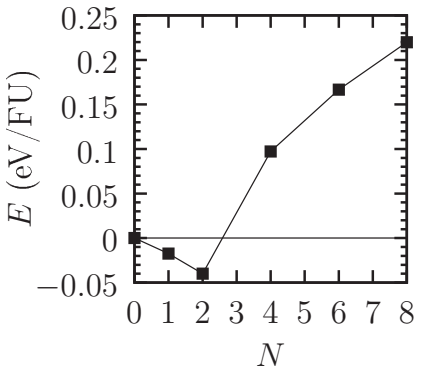

FIG. 14. Total energy (per formula unit) of the pyrite (100)–marcasite (101)–vacuum supercell as a function of the number of epitaxial layers of marcasite, N. The total energies are referenced to a clean pyrite (100) surface ($N = 0$). The global minimum is obtained when $N = 2$.

Although a trace amount of marcasite is predicted to be present, and is indeed observed experimentally,[9,25] whether it really affects the photovoltaic performance of pyrite is a separate issue. Electronic structure calculations of the two phases are presented in the following subsection.

C. Difference in bulk band gaps

Whether the presence of marcasite affects the OCV of pyrite depends on (i) the band gaps of the two phases, and (ii) the position of interfacial states. Here we discuss the issue of band gaps (i). Interfacial states (ii) are discussed in Sec. V D. The

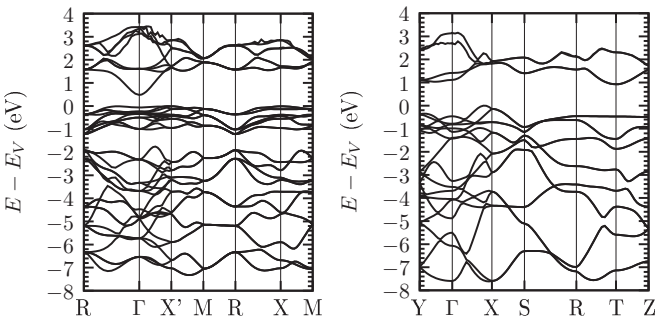

FIG. 15. PBE band structure of (a) pyrite and (b) marcasite. Both of them are indirect-gap materials. High symmetry points correspond to those in Ref. 28. The LDA and AM05 band structures look very similar and are not shown.

TABLE III. Band gap (in eV) and k-points at VB and CB edges. HSE06 and Δ-sol gaps are obtained at the experimental lattice constants.

	Pyrite			Marcasite		
	E_g	VB	CB	E_g	VB	CB
LDA	0.22	(0.4375,0,0)	(0,0,0)	0.88	(0.375,0,0)	(0,0.5,0.5)
PBE	0.40	(0.4375,0,0)	(0,0,0)	0.81	(0.4375,0,0)	(0,0.5,0.5)
PBE+U	1.03	(0.4375,0,0)	(0,0,0)	1.18	(0.4375,0,0)	(0,0.5,0.5)
AM05	0.29	(0.4375,0,0)	(0,0,0)	0.88	(0.375,0,0)	(0,0.5,0.5)
AM05+U	0.72	(0.4375,0,0)	(0,0,0)	1.18	(0.375,0,0)	(0,0.5,0.5)
HSE06	2.76	(0.5,0.5,0)	(0,0,0)	2.72	(0.5,0,0)	(0,0.5,0)
Δ-sol	1.3			1.2		
Experiment	0.95[a]			0.34[b]		

[a]Reference 2.
[b]Reference 27.

PBE band structures of pyrite and marcasite are compared in Fig. 15. The band gaps and critical k points are listed in Table III. For pyrite, the CB edge is located at the Γ point. The VB between 0 and −1.5 eV is very flat, indicating that the states are highly localized, as seen in the DOS in Fig. 9. The VB edge is located along the high-symmetry Δ line, which connects Γ and X'. However, we note that the direct transition at Γ is only 0.08 eV larger than the indirect gap, in agreement with the experimental difference (1.03 eV for direct transition versus 0.95 eV for indirect transition).[2] For marcasite, the CB edge is located at (0,0.5,0.5), while the VB edge occurs along the Σ line. Comparing the lowest conduction bands of pyrite and marcasite at the Γ point, the sharp minimum in pyrite is not seen in marcasite. Based on the DOS (Fig. 9), the character of the band in pyrite is an S p state, whose presence leads to the CB tail. Such a state is not found in marcasite (Fig. 16). Across all functionals that are used (Table III), the Kohn-Sham gap of marcasite is at least comparable to that of pyrite, and significantly higher than the estimate for the experimental gap of 0.34 eV.[27]

It is well known that the first-principles KS gap in local and semilocal functionals severely underestimates the band gap. Therefore, we have also calculated the band gaps using two other approaches that have been reported to be more accurate. The hybrid functional Heyd-Scuseria-Ernzerhof (HSE06),[55–58] which has been shown to produce accurate band gaps for solids, gives 2.8 (2.7) eV for pyrite (marcasite). The Δ-sol method, a recently developed total-energy method based on dielectric screening,[59] gives 1.3 (1.2) eV for pyrite (marcasite). In both methods, the pyrite and marcasite gaps are almost the same. In the Δ-sol method, the marcasite gap is predicted to be almost 0.9 eV larger than the experimental value,[27] although the pyrite gap is only slightly (0.3 eV) larger than the experimental value.[2]

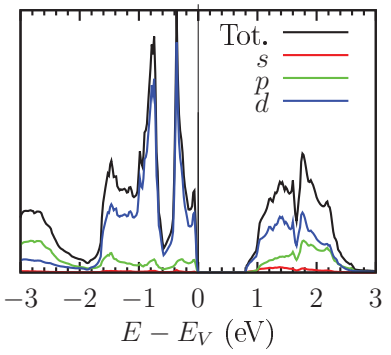

FIG. 16. (Color online) DOS of bulk marcasite within the GGA-PBE. Contrary to pyrite, there are no pronounced tail states at the CB in marcasite.

D. Absence of interfacial states within the band gap

Apart from the band-gap issue, we also examine the DOS at the pyrite-marcasite interface constructed from the lowest-energy configuration [corner-sharing interface, $\theta = 270°$)] to see if interfacial states are present that can pin the Fermi level. The DOS of the $N = 10$ and $\theta = 270°$ pyrite-marcasite interface is shown in Fig. 17. Two important observations are made. First, the band gap of the pyrite-marcasite supercell is the minimum of the pyrite and marcasite bulk band gaps. It is not smaller than the pyrite gap. Second, no interfacial states are seen within the band gap. From these results, we conclude that, although marcasite is present at trace amounts under thermodynamic conditions, its electronic structure does not undermine the photovoltaic performance of pyrite.

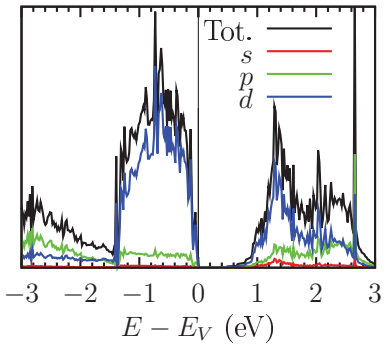

FIG. 17. (Color online) DOS of the lowest-energy pyrite (100)–marcasite (101) interface (corner-sharing, $\theta = 270°$) within the GGA-PBE. By comparing to Fig. 9, two key observations are made: (i) the band gap is not reduced; (ii) gap states are not found.

VI. DISCUSSION

As mentioned in Sec. II C 1, the ligand field model of Bronold *et al*. involves an unknown parameter ρ. For Bronold's choice of $\rho = 2$, two gap states are predicted within the gap. However, for $\rho = 1$, the splitting energy between a_1 (d_{z^2}) and b_2 (d_{xy}) states becomes 5.14 Dq,[18] or 1.03 eV, which is larger than the experimental band gap of pyrite. This implies that whether the intrinsic surface states are gap states or not depends on the choice of ρ. Our first-principles calculations reveal that the surface states are located near the band edge or deep within the band, with a splitting energy around 1.2 eV within PBE+U [Fig. 10(b)], resembling more closely the $\rho = 1$ scenario than the $\rho = 2$ scenario. Hence, the conclusion made by Bronold *et al*.[5] regarding gap states may be unfounded as it is based on an uncontrolled assumption for ρ.

The absence of gap states in the (100) surface of pyrite is confirmed by another first-principles study conducted by Cai and Philpott.[8] Although two other first-principles studies have observed gap states,[7,13] their results do not validate the Bronold model. (i) In the study by Oertzen *et al*.,[13] the origin of gap states is not due to *intrinsic* surface states, but is due to an additional half monolayer of S atoms on the otherwise properly terminated surface. (ii) In the study by Qiu *et al*.,[7] only one type of Fe d gap state is observed, contrary to the prediction of two types of gap states of d_{z^2} and d_{xy} characters by Bronold *et al*.[5] It should be pointed out that the position of the d_{z^2} surface state is susceptible to errors in the exchange-correlation functional. Although its relative position with respect to the VB has a wide range, being from 0.2 eV in the LDA to 1 eV in PBE+U, we find that it remains within the CB across all functionals. Since the Hubbard U model is designed to correct for localized d and f states,[60] the fact that the localized d_{z^2} intrinsic surface state is contained above the CBM within PBE+U, as well as the uncorrected LDA, gives strong evidence that it is not a gap state.

Regardless of the apparent discrepancy among first-principles calculations in the literature, surface states may not be relevant under experimental conditions, as the pyrite surface is passivated by adsorbates from the electrolyte. Indeed, the DOS of a passivated pyrite (100) surface shows the depletion of antibonding surface states. This surface passivation effect has been observed by calculations using a monolayer of H, F, and Cl adsorbates on pyrite (100). For example, the PBE DOS of a Cl-adsorbed (100) surface is shown in Fig. 18. Compared to the DOS of the clean pyrite (100) surface [Fig. 9(b)], the intrinsic surface states at the bottom of the CB are no longer observed. Our results suggest that intrinsic surface states can be passivated. Experimentally, pyrite is often immersed in an aqueous halide (especially the iodide redox couple) in a photoelectrochemical cell, and surface passivation may occur spontaneously.[2] Thus, whether intrinsic surface states are gap states may not pertain to the photovoltaic performance of pyrite at the device level.

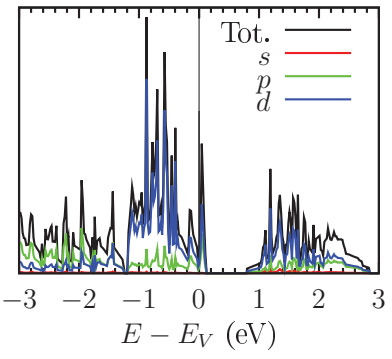

FIG. 18. (Color online) DOS of pyrite (100) with Cl adsorbates. The intrinsic surface state at the CB edge in Fig. 9(b) is depleted due to surface passivation.

From the energy model of marcasite epitaxial growth on pyrite [Eq. (1)], with first-principles total energies as input, we find that marcasite growth on pyrite is thermodynamically limited to one layer. This result is validated by direct computation of pyrite-marcasite-vacuum supercells, from which an additional layer of growth is stabilized by further ionic relaxation in the marcasite phase. Qualitatively, our prediction of a few layers of marcasite growth is verified by the experimental observation of a trace amount of marcasite after 46 h of XRD measuring time for 100 nm samples, but undetectable for thicker samples.[25] As our interfacial energy is well converged, the critical N is independent of the thickness of the pyrite substrate at the scale of the experimental sample. The volume percentage of marcasite in thin 100 nm samples is merely a fraction of 1%. Since our model predicts that the same amount of marcasite should form on the pyrite surface, the volume fraction of marcasite is smaller in thicker pyrite samples, eventually dropping below the threshold for detection.

Although limited marcasite growth is thermodynamically favorable, the critical question is whether marcasite affects the OCV of pyrite at all. Based on our calculation results, the marcasite Kohn-Sham gap is not smaller than the pyrite gap in any of the functionals that we used. Even though KS gaps of local and semilocal functionals are known to severely underestimate band gaps, the marcasite KS gaps obtained from such functionals are all larger than the reported experimental value, which leads us to suspect that the extraction of the marcasite gap from resistivity measurement[27] may not be an accurate determination of the band gap. As far as the authors are aware, the 0.34 eV marcasite gap is the only value reported and cited in the literature. If the marcasite gap is not smaller, but larger than the pyrite gap, as our result suggests, then its presence does not explain the low OCV of pyrite, contrary to the claim of Wadia *et al*.[9] We call for a more reliable experimental investigation (e.g., optical measurements) on the marcasite band gap. Moreover, from our interfacial calculations, the gap of pyrite is not reduced in the pyrite-marcasite system, and no gap states are found from the DOS (Fig. 17). However, we do not rule out the possibility of the formation of low-energy defect states at the interface. As we have not considered the role of native bulk, interfacial, or extrinsic defects in this study, further investigation is required to understand the cause of the low OCV of pyrite.

The theoretical limit in the OCV of any semiconductor can be calculated from the Shockley-Queisser equations.[61] The voltage ratio, defined as $v = qV_{oc}/E_g$, can be expressed analytically as a function of E_g. We plot $v(E_g)$ in Fig. 19. For pyrite, then, the theoretical OCV is 0.71 eV, which is more

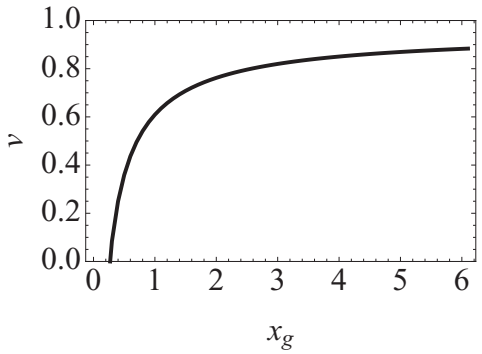

FIG. 19. Voltage ratio ($v = qV_{oc}/E_g$) as a function of $x_g = E_g/kT_s \approx 1.93E_g$, where $T_s = 6000$ K is the temperature of the sun, predicted by Shockley-Queisser theory.[62]

than three times the maximum experimental value of 0.2 eV.[2] In this study, we have established that the low OCV of pyrite cannot be explained by bulk or intrinsic surface properties. Moreover, the formation of marcasite is limited and gap states are not observed from electronic structure calculations of the pyrite-marcasite interface. The low OCV is likely to be caused by effects that we have not yet considered, e.g., defects.

From our band-structure calculation, another important issue that may have been overlooked is the low hole mobility of pyrite. Based on the curvature of the DFT band edge [Fig. 15(a)], pyrite is predicted to have very heavy holes. The flatness of the VB has previously been reported. For example, the pyrite band structure calculated by a linear combination of atomic orbitals (LCAO) can be found in Ref. 28; a DFT calculation is presented in Ref. 13. Our first-principles prediction that pyrite has low hole mobility is confirmed experimentally by Oertel *et al.*, who reported $\mu_p < 0.1$ cm^2/(V s).[15] In light of the strained silicon technology (see, e.g., Ref. 62 and references therein), one possible way to enhance the carrier mobility is to intentionally impose strain on pyrite thin films.

VII. CONCLUSIONS

Using first-principles computations, we have shown that two of the widely accepted reasons for the low OCV of pyrite photovoltaic devices are questionable. Although Bronold *et al.* have correctly predicted that broken symmetry on the pyrite surface causes intrinsic surface states,[5] the character and position are not reproduced within DFT. First, their predicted d_{xy} state is not observed to move out of the VB, and ligand field splitting of the VB is not seen. Second, no gap states are found. The only surface-induced state is the d_{z^2} state located at the CB edge, but the d_{xy} state remains within the VB.

Next, we have examined the claim that marcasite reduces the OCV of pyrite. To investigate the thermodynamic condition for the epitaxial growth of marcasite on pyrite, we have derived a parameter-free energy-balance equation [Eq. (1)] that involves the bulk, surface, interfacial, and strain energies of the two phases as input. Although a few layers of marcasite growth are predicted to be thermodynamically favorable, by examining the DOS at the pyrite-marcasite interface, no gap states are found. The marcasite gap is at least comparable to the pyrite gap, and significantly greater than the experimental marcasite gap, within all functionals used, suggesting that the experimental resistivity measurement of the marcasite gap[27] may need to be verified by more careful and reliable studies.

Although the direct cause of the low OCV of pyrite photovoltaic devices has not yet been established, we believe that the effects of intrinsic surface states and marcasite are at best secondary. Future work will focus on native and extrinsic defects.

ACKNOWLEDGMENTS

The authors thank Rickard Armiento, ShinYoung Kang, Predrag Lazic, and Yabi Wu for helpful discussions. R.S. and M.K.Y.C. were partially funded by the Chesonis Family Foundation under the Solar Revolution Project. R.S. was also funded by the Department of Energy under Contract No. DE-FG02-96ER45571. This research was supported in part by the National Science Foundation through TeraGrid resources provided by Texas Advanced Computing Center (TACC) under Grant No. TG-DMR970008S.

APPENDIX A: CALCULATION METHOD FOR SURFACE AND INTERFACIAL ENERGIES

Surface energies were calculated from the equation

$$\gamma = \lim_{N\to\infty} \frac{E^N_{\text{slab}} - N E_{\text{bulk}}}{2A}, \tag{A1}$$

where E^N_{slab} and E_{bulk} are the total energies of the slab and bulk, respectively, N is the supercell size, $A = ||\mathbf{T}_1 \times \mathbf{T}_2||$ is the cross-sectional area of the supercell ($\mathbf{T}_i$ is the translation vector along the i direction, where $i = 1,2,3$ corresponds to x,y,z), and the factor of 2 accounts for the presence of two surfaces under periodic boundary conditions. Surface energies were relaxed and converged to within 0.01 J/m^2 with respect to the number of layers and vacuum size (Table IV).

The interfacial energy between two phases α and β can be calculated from

$$\gamma_{\alpha\beta} = \lim_{N_\alpha, N_\beta\to\infty} \frac{E^{N_\alpha+N_\beta}_{\text{int}} - N_\alpha E^{\alpha}_{\text{bulk}} - N_\beta E^{\beta}_{\text{bulk}}}{2A}, \tag{A2}$$

where N denotes the number of layers for each phase. However, due to different cell shapes and k-point densities, it may be inaccurate to use the bulk energies obtained from conventional unit-cell calculations as reference energies for the

TABLE IV. Slab and vacuum size used to obtain pyrite surface energies. Here we define a unit cell as the smallest orthorhombic cell whose basal plane is the desired surface. The number of repetitions of such a cell along the z direction is denoted by N. This should not be confused with the definition of the number of [S-Fe-S] layers in Sec. V.

Surface	N	Vacuum size (Å)
(100)	2	6
(110)	2	8
(111)	1	6
(210)	1	8

TABLE V. Lattice constants and relative stability of pyrite and marcasite. Within the LDA and AM05, pyrite is the ground state, in agreement with experiment.[18] Within the GGA-PBE, marcasite is the ground state. However, as pressure is increased, the volumes of the two phases decrease, and pyrite becomes more energetically favorable relative to marcasite. Within HSE06, pyrite is 5.2 meV/FU more stable than marcasite at the experimental lattice constants.

		Pyrite		Marcasite				
	P (GPa)	a (Å)	V (Å^3)	a (Å)	b (Å)	c (Å)	V (Å^3)	$E_p - E_m$ (meV/FU)
Experiment[a]		5.416	158.9	4.443	5.425	3.387	81.64	−43.4
LDA	0	5.2875	147.82	4.3374	5.2974	3.3201	76.284	−8.4
AM05	0	5.3171	150.33	4.3615	5.3283	3.3415	77.653	−8.8
AM05+U	0	5.3325	151.32	4.3599	5.3323	3.3491	77.859	7.1
PBE	0	5.4029	157.72	4.4382	5.4094	3.3884	81.350	21.6
	2	5.3806	155.77	4.4164	5.3882	3.3753	80.321	6.3
	4	5.3605	154.03	4.3954	5.3682	3.3624	79.338	−8.6
	6	5.3406	152.32	4.3778	5.3491	3.3499	78.446	−23.1
	8	5.3212	150.67	4.3598	5.3309	3.3378	77.575	−37.3
	10	5.3048	149.29	4.3431	5.3139	3.3265	76.772	−51.1
PBE+U	0	5.4239	159.56	4.4373	5.4209	3.4068	81.949	24.9

[a]Lattice constants are taken from Ref. 1 (pyrite) and Ref. 20 (marcasite). Enthalpies of formation at 298.15 K are taken from Ref. 20.

supercells. Instead, one can obtain the average bulk reference energy, E_b, by fitting the total energy of the interface supercell versus the number of layers with a straight line, in the fashion developed by Fiorentini and Methfessel.[54] Note that when $N = N_\alpha = N_\beta$,

$$E_{\text{int}}^{2N} \approx 2\gamma_{\alpha\beta} A + N E_{\text{bulk}}. \tag{A3}$$

The bulk reference energy E_{bulk} must be fitted separately for each θ and parity of N. Substituting the fitted E_{bulk} into Eq. (A2), γ can be obtained as a function of N.

We use the Fiorentini-Methfessel method[54] to obtain the interfacial energy between marcasite and pyrite. The marcasite (101) cell is strained such that $a' \equiv \sqrt{a_m^2 + c_m^2} = a_p, b_m = a_p$, and $c/a = 1$, as discussed in the main text. By inserting a vacuum layer to this cell, the marcasite (101) surface energy is calculated to be 0.72 J/m^2. The corresponding strain energies within the GGA-PBE are given in Table II. The strain energies are on the order of 100 meV/FU, much higher than the relative stability energy between the two phases, which is on the order of 10 meV/FU, from Table V.

APPENDIX B: VOLUME DEPENDENCE OF THE RELATIVE STABILITY OF PYRITE AND MARCASITE

From total energy calculations of the bulk phases, we find that the thermodynamic ground state is marcasite in PBE and PBE+U, but pyrite in LDA and AM05. As shown in Table V, pyrite is 21.6 meV/FU less stable than marcasite within the GGA-PBE, but 8 meV/FU more stable within the LDA and AM05. These results agree with the relative stability reported by Spagnoli *et al.*,[10] except for the LDA calculation. They report that marcasite is the ground state within the LDA, with a relative energy difference of 31 meV/FU.[10] However, we find that pyrite is the ground state within the LDA. To verify whether the prediction of the relative phase stability is simply a volume issue, we plot in Fig. 20 the PBE energy difference between pyrite and marcasite as a function of pressure. For pressures larger than 2.8 GPa, pyrite is favored. At this critical pressure, the conventional cell volumes of pyrite and marcasite are expected to be about 155 and 80 Å^3, respectively, which are higher than the equilibrium volumes within the LDA and AM05. Upon further increase in pressure until $P = 4$ GPa, the volumes are reduced and the energy difference (−8.6 meV/FU) coincides with the $P = 0$ calculations within the LDA and AM05. Hence, prediction of the relative stability can be corrected by decreasing the volume, either by artificially applying a pressure within PBE, or using the LDA/GGA-AM05.

We remark that the lattice constant calculated within the GGA-PBE is underestimated compared to experiment, which is unusual. Extrapolation of the experimental lattice constant of pyrite using its thermal expansion coefficient[63] yields about 5.41 Å at 0 K, which is still 0.2% larger than the PBE lattice constant at zero pressure, and 2% larger than the LDA lattice constant. Thus, there is a trade-off between the prediction of relative stability and equilibrium volume. In particular, while the AM05+U ($U_{\text{eff}} = 2$ eV) lattice constants and band gap (Table III) show better agreement with the experimental values, the ground-state phase is predicted to be marcasite. All LDA,

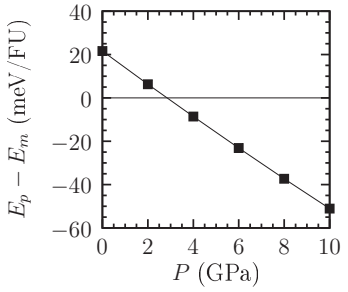

FIG. 20. Relative stability of pyrite and marcasite as a function of applied pressure within GGA-PBE. The crossover occurs at 2.8 GPa. To reach the same relative stability predicted by the LDA and AM05 ($E_p - E_m = -8.6$ meV/FU), a pressure of 4 GPa is needed.

PBE, and AM05 calculations presented in the main text are performed at the equilibrium lattice constant corresponding to the functional being used.

Our work shows that qualitative trends in the electronic structure are independent of the functionals considered, and that either the LDA, AM05, or HSE06 can be used to predict the correct bulk ground-state phase. At the pyrite-marcasite interface, the DOS plots and interfacial energies are consistent across functionals. The functional dependence of properties that have not been studied in this work (e.g., phonon) is unknown. We have made an effort to illustrate that while relative stability and volume depend on the functional, the electronic properties pertaining to the photovoltaic performance of pyrite do not.

*gceder@mit.edu

[1] R. Murphy and D. R. Strongin, Surf. Sci. Rep. **64**, 1 (2009).
[2] A. Ennaoui, S. Fiechter, C. Pettenkofer, N. Alonso-Vante, K. Büker, M. Bronold, C. Höpfner, and H. Tributsch, Sol. Energy Mater. Sol. Cells **29**, 289 (1993).
[3] I. Ferrer, D. Nevskaia, C. de las Heras, and C. Sanchez, Solid State Commun. **74**, 913 (1990).
[4] C. Wadia, A. P. Alivisatos, and D. M. Kammen, Environ. Sci. Technol. **43**, 2072 (2009).
[5] M. Bronold, Y. Tomm, and W. Jaegermann, Surf. Sci. **314**, L931 (1994).
[6] M. Bronold, K. Büker, S. Kubala, C. Pettenkofer, and H. Tributsch, Phys. Status Solidi A **135**, 231 (1993).
[7] Q. Guanzhou, X. Qi, and H. Yuehua, Comput. Mater. Sci. **29**, 89 (2004).
[8] J. Cai and M. R. Philpott, Comput. Mater. Sci. **30**, 358 (2004).
[9] C. Wadia, Y. Wu, S. Gul, S. K. Volkman, J. Guo, and A. P. Alivisatos, Chem. Mater. **21**, 2568 (2009).
[10] D. Spagnoli, K. Refson, K. Wright, and J. D. Gale, Phys. Rev. B **81**, 094106 (2010).
[11] M. Birkholz, S. Fiechter, A. Hartmann, and H. Tributsch, Phys. Rev. B **43**, 11926 (1991).
[12] M. Bronold, C. Pettenkofer, and W. Jaegermann, J. Appl. Phys. **76**, 5800 (1994).
[13] G. U. von Oertzen, W. M. Skinner, and H. W. Nesbitt, Phys. Rev. B **72**, 235427 (2005).
[14] A. Abd El Halim, S. Fiechter, and H. Tributsch, Electrochim. Acta **47**, 2615 (2002).
[15] J. Oertel, K. Ellmer, W. Bohne, J. Röhrich, and H. Tributsch, J. Cryst. Growth **198-199**, 1205 (1999).
[16] S. Harmer and H. Nesbitt, Surf. Sci. **564**, 38 (2004).
[17] M. Koichi and I. Fujio, J. Appl. Crystallogr. **41**, 653 (2008).
[18] R. Krishnamurthy and W. Schaap, J. Chem. Educ. **47**, 433 (1970).
[19] F. Hulliger and E. Mooser, J. Phys. Chem. Solids **26**, 429 (1965).
[20] F. Grønvold and E. Westrum Jr., J. Chem. Thermodyn. **8**, 1039 (1976).
[21] B. Hyde and M. O'Keeffe, Aust. J. Chem. **49**, 867 (1996).
[22] M. E. Fleet, Can. Mineral. **10**, 225 (1970).
[23] K. J. Brock and L. J. Slater, Am. Mineral. **63**, 210 (1978).
[24] D. Schleich and H. Chang, J. Cryst. Growth **112**, 737 (1991).
[25] B. Thomas, T. Cibik, C. Höpfner, K. Diesner, G. Ehlers, S. Fiechter, and K. Ellmer, J. Mater. Sci.: Mater. Electron. **9**, 61 (1998).
[26] W. Folkerts, G. Sawatzky, C. Haas, R. Groot, and F. Hillebrecht, J. Phys. C **20**, 4135 (1987).
[27] M. Jagadeesh and M. Seehra, Phys. Lett. A **80**, 59 (1980).
[28] D. Bullett, J. Phys. C **15**, 6163 (1982).
[29] P. Hohenberg and W. Kohn, Phys. Rev. **136**, B864 (1964).
[30] W. Kohn and L. J. Sham, Phys. Rev. **140**, A1133 (1965).
[31] P. E. Blöchl, Phys. Rev. B **50**, 17953 (1994).
[32] G. Kresse and D. Joubert, Phys. Rev. B **59**, 1758 (1999).
[33] G. Kresse and J. Hafner, Phys. Rev. B **47**, 558 (1993).
[34] G. Kresse and J. Hafner, Phys. Rev. B **49**, 14251 (1994).
[35] G. Kresse and J. Furthmüller, Phys. Rev. B **54**, 11169 (1996).
[36] G. Kresse and J. Furthmüller, Comput. Mater. Sci. **6**, 15 (1996).
[37] J. P. Perdew and A. Zunger, Phys. Rev. B **23**, 5048 (1981).
[38] J. P. Perdew, K. Burke, and M. Ernzerhof, Phys. Rev. Lett. **77**, 3865 (1996).
[39] J. P. Perdew, K. Burke, and M. Ernzerhof, Phys. Rev. Lett. **78**, 1396 (1997).
[40] R. Armiento and A. E. Mattsson, Phys. Rev. B **72**, 085108 (2005).
[41] A. E. Mattsson and R. Armiento, Phys. Rev. B **79**, 155101 (2009).
[42] U. von Barth and L. Hedin, J. Phys. C **5**, 1629 (1972).
[43] M. M. Pant and A. K. Rajagopal, Solid State Commun. **10**, 1157 (1972).
[44] A. I. Liechtenstein, V. I. Anisimov, and J. Zaanen, Phys. Rev. B **52**, R5467 (1995).
[45] K. Persson, G. Ceder, and D. Morgan, Phys. Rev. B **73**, 115201 (2006).
[46] H. J. Monkhors and J. D. Pack, Phys. Rev. B **13**, 5188 (1976).
[47] P. Tasker, J. Phys. C **12**, 4977 (1979).
[48] A. Hung, J. Muscat, I. Yarovsky, and S. P. Russo, Surf. Sci. **513**, 511 (2002).
[49] A. Hung, J. Muscat, I. Yarovsky, and S. P. Russo, Surf. Sci. **520**, 111 (2002).
[50] D. Alfonso, J. Phys. Chem. C **114**, 8971 (2010).
[51] V. Eyert, K.-H. Höck, S. Fiechter, and H. Tributsch, Phys. Rev. B **57**, 6350 (1998).
[52] H. J. Kulik, M. Cococcioni, D. A. Scherlis, and N. Marzari, Phys. Rev. Lett. **97**, 103001 (2006).
[53] L. Wang, T. Maxisch, and G. Ceder, Phys. Rev. B **73**, 195107 (2006).
[54] V. Fiorentini and M. Methfessel, J. Phys. Condens. Matter **8**, 6525 (1996).
[55] J. Heyd, G. E. Scuseria, and M. Ernzerhof, J. Chem. Phys. **118**, 8207 (2003).
[56] J. Heyd, G. E. Scuseria, and M. Ernzerhof, J. Chem. Phys. **124**, 219906 (2006).
[57] J. Paier, M. Marsman, K. Hummer, G. Kresse, I. C. Gerber, and J. G. Angyan, J. Chem. Phys. **124**, 154709 (2006).
[58] J. Paier, M. Marsman, K. Hummer, G. Kresse, I. C. Gerber, and J. G. Angyan, J. Chem. Phys. **125**, 249901 (2006).
[59] M. K. Y. Chan and G. Ceder, Phys. Rev. Lett. **105**, 196403 (2010).
[60] V. I. Anisimov, F. Aryasetiawan, and A. I. Lichtenstein, J. Phys. Condens. Matter **9**, 767 (1997).
[61] W. Shockley and H. Queisser, J. Appl. Phys. **32**, 510 (1961).
[62] Y. Sun, S. E. Thompson, and T. Nishida, J. Appl. Phys. **101**, 104503 (2007).
[63] G. Willeke, O. Blenk, C. Kloc, and E. Bucher, J. Alloys Compd. **178**, 181 (1992).